Taylor & Francis
Taylor & Francis Group

Xenobiotica
the fate of foreign compounds in biological systems

ISSN: 0049-8254 (Print) 1366-5928 (Online) Journal homepage: http://www.tandfonline.com/loi/ixen20

Pharmacokinetics, metabolism, and excretion of nefopam, a dual reuptake inhibitor in healthy male volunteers

Madhu Sanga, John Banach, Aaron Ledvina, Nishit B. Modi & Aravind Mittur

To cite this article: Madhu Sanga, John Banach, Aaron Ledvina, Nishit B. Modi & Aravind Mittur (2016): Pharmacokinetics, metabolism, and excretion of nefopam, a dual reuptake inhibitor in healthy male volunteers, Xenobiotica, DOI: 10.3109/00498254.2015.1136989

To link to this article: http://dx.doi.org/10.3109/00498254.2015.1136989

http://informahealthcare.com/xen
ISSN: 0049-8254 (print), 1366-5928 (electronic)

Xenobiotica

Xenobiotica, Early Online: 1–16
 DOI: 10.3109/00498254.2015.1136989

Taylor & Francis
Taylor & Francis Group

RESEARCH ARTICLE

Pharmacokinetics, metabolism, and excretion of nefopam, a dual reuptake inhibitor in healthy male volunteers

Madhu Sanga[1*], John Banach[1*], Aaron Ledvina[1*], Nishit B. Modi[2], and Aravind Mittur[2]

[1]*Covance Laboratories Inc, Madison, WI, USA and* [2]*Department of Clinical Pharmacology, Impax Specialty Pharma (A Division of Impax Laboratories, Inc.), Hayward, CA, USA*

Abstract

1. The disposition of nefopam, a serotonin–norepinephrine reuptake inhibitor, was characterized in eight healthy male volunteers following a single oral dose of 75 mg [^{14}C]-nefopam (100 μCi). Blood, urine, and feces were sampled for 168 h post-dose.
2. Mean (± SD) maximum blood and plasma radioactivity concentrations were 359 ± 34.2 and 638 ± 64.7 ngEq free base/g, respectively, at 2 h post-dose. Recovery of radioactive dose was complete (mean 92.6%); a mean of 79.3% and 13.4% of the dose was recovered in urine and feces, respectively.
3. Three main radioactive peaks were observed in plasma (metabolites M2 A-D, M61, and M63). Intact [^{14}C]-nefopam was less than 5% of the total radioactivity in plasma. In urine, the major metabolites were M63, M2 A-D, and M51 which accounted for 22.9%, 9.8%, and 8.1% of the dose, respectively. An unknown entity, M55, was the major metabolite in feces (4.6% of dose). Excretion of unchanged [^{14}C]-nefopam was minimal.

Keywords

Human disposition, mass balance, metabolite profiling and identification, radiolabeled nefopam

History

Received 20 November 2015
Revised 24 December 2015
Accepted 26 December 2015
Published online 20 January 2016

Introduction

Racemic nefopam [(±)-3,4,5,6-tetrahydro-5-methyl-1-phenyl-1H-2,5-benzoxazocine hydrochloride] (Figure 1) is a potent centrally acting non-opioid analgesic. Nefopam is a mixture of two enantiomers: (+)*S*- and (−)*R*-nefopam, and is used for the treatment of moderate to severe acute and chronic pain. It also exhibits antidepressant activity in non-clinical models (Bolt et al., 1974). Its mode of action in analgesia likely involves inhibition of the synaptosomal reuptake of norepinephrine and serotonin, and increased neurotransmission in descending pain inhibitory pathways (Hunskaar et al., 1987). Antinociception mediated by nefopam may also involve the glutamatergic pathway by modulation of the voltage-sensitive calcium and sodium channels (Novelli et al., 2005; Verleye et al., 2004). Nefopam has weaker affinity to serotonergic 5-HT$_{2C}$, 5-HT$_{2A}$, 5-HT$_3$, 5-HT$_{1B}$, 5-HT$_{1A}$, and α adrenergic receptors (Girard et al., 2006).

Nefopam has potential therapeutic uses in multiple indications. Inhibitors of serotonin and norepinephrine reuptake (SNRI) are a mainstay in the therapy of disorders including major depression, anxiety disorders, and various chronic pain disorders such as fibromyalgia and neuropathic pain. Prototype SNRIs include venlafaxine, duloxetine, milnacipran, and levomilnacipran. The clinical advantages and limitations of SNRIs have been reviewed (Dell'Osso et al., 2010; Lee & Chen, 2010; Taylor et al., 2013; Thase, 2008).

Following a single intravenous (IV) dose of radiolabeled nefopam in healthy human subjects, 87% of the dose is excreted in urine within 5 d and 8% in feces (Heel et al., 1980). Less than 5% of a single IV or oral dose of nefopam is excreted in urine as unchanged parent, suggesting extensive hepatic metabolism (Chawla et al., 2003). Peak plasma concentration (C_{max}) of nefopam is attained 1–2 h after an oral dose and is eliminated with an apparent terminal half-life ($t_{1/2}$) of 3–8 h. Seven metabolites have been observed in man including desmethyl nefopam, nefopam *N*-oxide, and its *N*-glucuronide, a majority of which are excreted in urine (Heel et al., 1980). However, the complete biotransformation of nefopam and its metabolite profile is unknown. The absolute oral bioavailability of nefopam in humans is low (Aymard et al., 2003). Following IV nefopam, on one hand, plasma concentrations of *N*-desmethyl nefopam are much lower than nefopam and peak later (5.1 h) than after an oral dose. On the other hand, plasma concentrations of *N*-desmethyl nefopam (and its enantiomers) following oral nefopam reach a maximum at 2.5 h and approach that of nefopam (Aymard et al., 2003). The apparent $t_{1/2}$ of *N*-desmethyl nefopam is longer (10–15 h) than nefopam indicating that half-life is elimination-rate limited rather than formation-rate limited. These findings suggest that at least some of the desmethyl

*Current address: Alcon Research, Ltd., Fort Worth, TX, USA.

Address for correspondence: Aravind Mittur, PhD, Clinical Pharmacology, Impax Specialty Pharma, 31047 Genstar Road, Hayward, CA 94544, USA. Tel: +1 510 240 6437. E-mail: amittur@impaxlabs.com

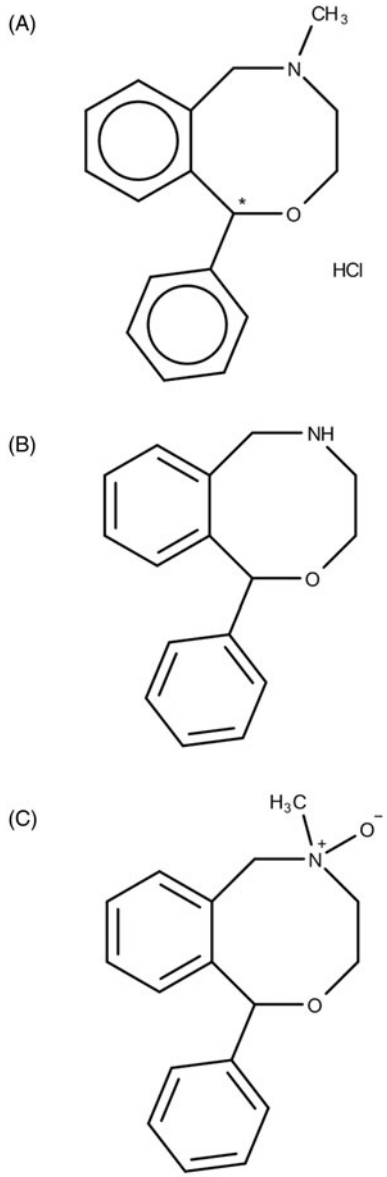

Figure 1. Structures of (A) nefopam HCl (5-methyl-1-phenyl-1,3,4,6-tetrahydro-2,5-benzoxazocine), (B) *N*-desmethyl nefopam HCl, and (C) (lR,5R)/(lS,5S)-nefopam *N*-oxide. *The site of radiolabeled carbon.

metabolites are generated during the absorption process, i.e., intestinal first-pass effect (Houston & Taylor, 1984). Approximately 73% of nefopam is protein bound in human plasma over a range of 7–226 ng/mL. Slower metabolism and excretion of IV nefopam have been reported in subjects with renal dysfunction (Mimoz et al., 2010).

The pharmacological effects of the metabolites of nefopam have not been established. Racemic nefopam and desmethyl-nefopam are equipotent after subcutaneous, oral, and intraventricular administration in a rat model of analgesia (Kirchherr & Christ, 1984). Adverse effects of nefopam are transient and of moderate severity including sedation, drowsiness, sweating, tachycardia, nausea, dizziness, and pain at the injection site (Evans et al., 2008; Heel et al., 1980; Kapfer et al., 2005). Differential route-dependent clinical effects such as analgesia, sedation, and drowsiness have been attributed to metabolites (Aymard et al., 2003; Chawla et al., 2003). It is, therefore, of interest to estimate and relate the overall systemic exposure to nefopam-derived molecules in non-clinical toxicology and clinical studies.

Understanding the disposition and metabolism of nefopam in humans would help assess (1) a comprehensive picture of metabolites and their relative abundance, (2) the presence of potentially active metabolites, and (3) differences in systemic exposure to metabolites in non-clinical species and clinical studies. The present study sought to (1) examine mass balance in healthy male subjects after a single oral dose of 75 mg [^{14}C]-nefopam containing approximately 100 μCi of radioactivity administered as the hydrochloride (HCl) salt, (2) quantify nefopam and total radioactivity in plasma, urine and feces, (3) investigate the routes of elimination of nefopam, and (4) elucidate the biotransformation of nefopam by profiling and identifying its metabolites in various matrices.

Materials and methods

Chemicals and reference compounds

Nefopam HCl ((±)-3,4,5,6-tetrahydro-5-methyl-1-phenyl-1H-2,5-benzoxazocine hydrochloride) was supplied by Impax Laboratories (Hayward, CA). [^{14}C]-nefopam HCl (Figure 1A) was synthesized by Ricerca Biosciences LLC (Cleveland, OH). The optimal location of the radiolabel in nefopam was planned by incorporating the known human metabolites as well as considering all predicted metabolites and sites of metabolism by *in silico* analyses primarily using SMARTCyp (Rydberg et al., 2010). [^{14}C]-Nefopam HCl was assayed by HPLC coupled with radiometric detection and found to be 97% pure with a specific activity of 198.9 μCi/mg. Reference standards of *N*-desmethyl nefopam (Figure 1B) and (lR,5R)/(lS,5S)-nefopam *N*-oxide (Figure 1C) and their d4 deuterated forms were procured from TLC Pharmachem Inc. (Ontario, Canada). All other materials were of HPLC or analytical grade.

Clinical study design

This was an open-label, single-dose study conducted in eight non-smoking healthy male volunteers between the ages of 18 and 55 years, with a body mass index between 18.0 and 29.5 kg/m^2. The study protocol, consent documents, consent procedures, and subject recruitment procedures were approved by the Institutional Review Board. The study was conducted in full compliance with the Declaration of Helsinki and the International Conference on Harmonization Good Clinical Practices guidelines. All study participants provided written, informed consent before participation in the study. All subjects were genotyped for variants of CYP2D6 and CYP2C19. A single 6-mL sample of blood was collected prior to dosing. Subjects provided separate written informed consent for DNA collection and participation. Subjects were confined to the CRU at Covance Laboratories, Inc. (Madison, WI) under continuous observation approximately 12 h before dosing through at least 144 h postdose or until a minimum of 90% of the administered radioactive dose was recovered in excreta or less than 1% was excreted in a 24-h period for two consecutive 24-h intervals.

Study medication, dose formulation, and administration

Doses were prepared as a dry blend of both radiolabeled and unlabeled GMP nefopam HCl. The specific activity of the final blend was 1.17 μCi/mg with a purity of >98% by HPLC. Just before administration, the blended powder was dissolved in 20 mL sterile water for irrigation at the radiopharmacy in the Clinical Research Unit (CRU) of Covance Laboratories, Inc. (Madison, WI) to provide a target dose 75 mg of nefopam (free base equivalent) with approximately 100 μCi of radioactivity for each subject. Assayed samples were found to contain >99.7% of the target dose of nefopam (mass and radioactivity) and were ≥95% pure. Each subject was administered a single oral dose of [^{14}C]-nefopam HCl (75 mg free base equivalent; 100 μCi) in an aqueous solution (240 mL total volume including 20 mL dose solution, vial rinses, and residual water). The residual radioactivity in the rinsed dosing vials was determined and accounted for approximately 0.3% of the total radioactivity. Subjects were fasted for 8 h prior to and for 4 h after dose administration. Subjects were not allowed any beverages, other than water associated with dose administration, from 1 h prior to dosing and continuing up to 2 h after dosing. Subjects were prohibited from consuming grapefruit or grapefruit-related citrus fruits from 3 d prior to dosing until the collection of the final pharmacokinetics (PK) blood sample.

Sample collection

Venous blood samples (8 mL) were collected from each subject in tubes (containing K_2EDTA as an anticoagulant) predose (within 1 h prior to dosing), 0.5, 1, 2, 2.5, 3, 4, 5, 6, 9, 12, 16, 24, 32, 36, 48, 60, 72, 96, and 120 h postdose, and if subject did not meet discharge criteria at 144, 168, 192, and 216 h postdose. An aliquot of whole blood from these samples was stored at 4 °C for analysis of total radioactivity. Plasma was fractioned by centrifugation of residual blood and stored at −70 °C for bioanalysis of nefopam, *N*-desmethyl nefopam, and nefopam *N*-oxide by a validated bioanalytical method, and for quantitation of total radioactivity. One of the subjects was administered a single dose of 30 mg milk of magnesia to ensure defecation on day 7 (168 h), per protocol. Blood sample collections were terminated after 144 h postdose for this subject; however, the subject was not discharged from the study until 168 h postdose. Separately, up to 12 blood samples (8 mL each) were collected from each subject predose (within 1 h prior to dosing), 1, 2, 4, 6, 9, 12, 24, 48, 72, 96, and 120 h postdose for profiling and identification of metabolites. Plasma fractionated from these samples was stored at −70 °C. A sample of voided urine was collected before dosing and subsequently at intervals of 0–3, 3–6, 6–9, 9–12, 12–24, 24–36, 36–48, 48–60, and 60–72 h postdose. After 72 h, total voided urine was collected in 24-h intervals until discharge from the study. Urine samples were refrigerated at 4 °C until the end of each collection period, and the total weight and pH of urine were recorded. At the end of each collection period, two aliquots of urine (20 mL) were taken from each sample and stored in polypropylene tubes at −20 °C until analysis. Additionally, a 10 mL aliquot of urine from each collection period was stored at 4 °C for quantitation of total radioactivity. Feces were collected daily after dosing at 24-h intervals until discharge. Fecal samples were stored at −20 °C.

Quantitation of total radioactivity in blood, plasma, urine, and feces

Analysis of total radioactivity in blood, plasma, urine, and feces was conducted at Covance Laboratories, Inc. (Madison, WI). All sample combustions were done in a PerkinElmer Model 307 Sample Oxidizer (PerkinElmer, Boston, MA) and the resulting $^{14}CO_2$ was trapped in CarboSorb (Varian, Inc., Palo Alto, CA) and counted with Permafluor E (PerkinElmer, Boston, MA) as the scintillant. Oxidation efficiency was evaluated on each day of sample combustion by analyzing a commercial radiolabeled standard both directly in scintillation cocktail and by oxidation. Acceptance criteria were combustion recoveries of 95–105%. Ultima Gold XR was used as scintillation cocktail for samples analyzed directly. All samples were analyzed for radioactivity in a PerkinElmer Tri-Carb 2900TR liquid scintillation counter (LSC) (PerkinElmer, Boston, MA) for at least 5 min or 100 000 counts. Each sample was homogenized or mixed before radioanalysis (unless the entire sample was used for analysis). All samples were analyzed in duplicate if sample size allowed. Scintillation counts (CPM) were automatically corrected for counting efficiency using the external standardization technique and an instrument stored quench curve generated from a series of sealed quenched standards. Blood and plasma samples (approximately 0.2 g) were combusted and analyzed by LSC. Urine samples from each collection interval were aggregated at the CRU and the urine subsamples were mixed and duplicate weighed aliquots (approximately 0.2 g) were analyzed directly by LSC. The total weight and the pH of each urine sample were recorded at the CRU. Fecal samples from each subject were combined at 24-h intervals and the weight of each combined sample was recorded. A weighed amount of reverse osmosis (RO) water was added and the sample was mixed using a probe-type homogenizer. Duplicate weighed aliquots (approximately 0.2 g) were combusted and analyzed by LSC. Weighed subsamples (approximately 50 g) were transferred to properly labeled containers for metabolite profiling. Total radioactivity in blood and plasma was expressed as nanogram-equivalents (ng Eq free base)/g. The amount of total radioactivity (ng Eq) in urine and feces was determined by multiplying the volume or weight of the samples by the radioactivity concentration. For data values below the limit of quantification, a value of zero was assigned for calculations of means. Radioactivity recovered in urine and feces was expressed as a percentage of the total administered radioactivity as well as the amount excreted in mg equivalents. All calculations were based on the actual dose (71.9–72.1 mg, 96.3–96.6 μCi) administered to each subject. Any sample that was less than two times the background DPM was assigned a value of zero. The lower limit of quantitation (LLOQ) for total radioactivity in blood, plasma, urine, and feces was 35.3, 27.7, 29.4, and 138 ng Eq free base/g, respectively. The radioactivity in RBCs was estimated as a

percentage of total radioactivity in whole blood by the following equation:

$$\text{Radioactivity in RBC} = \frac{\left[C_b - \left(1 - \frac{Hct}{100}\right) \times C_p\right]}{C_b}$$

where C_b and C_p were the radioactivity concentrations in whole blood and plasma, respectively, and *Hct* was the hematocrit value obtained from predose blood sample and follow-up.

Quantitative bioanalysis

N-desmethyl nefopam and nefopam *N*-oxide were prospectively identified as metabolites of interest based on prior findings in the literature (Aymard et al., 2003; Heel et al., 1980). The concentrations of nefopam, *N*-desmethyl nefopam, and nefopam *N*-oxide in plasma and urine were determined at Covance Laboratories, Inc. (Madison, WI) using a validated LC-MS/MS assay. Nefopam, *N*-desmethyl nefopam, nefopam *N*-oxide, and the internal standards were extracted from samples using solid-phase extraction. Calibration response curves were linear over the range of 1.0–250 ng/mL for nefopam and *N*-desmethyl nefopam, and 5.0–250 ng/mL (2.5–250 ng/mL in urine) for nefopam *N*-oxide using a weighted (1/concentration^2) linear least-squares regression. The LLOQ in plasma for nefopam and *N*-desmethyl nefopam was 1.0 ng/mL and for nefopam *N*-oxide 5.0 ng/mL. The LLOQ in urine was 1.0 ng/mL for nefopam and *N*-desmethyl nefopam and 2.5 ng/mL for nefopam *N*-oxide. QC samples containing nefopam, *N*-desmethyl nefopam, and nefopam *N*-oxide at 3, 25, 200, and 5000 (dilution QC) ng/mL were run with the samples from the study. Dilution QC samples were also included in batches where samples needed to be diluted prior to analysis. The QC sample-relative standard deviations (RSD) ranged from 1.7 to 6.0% for nefopam, 1.8 to 4.3% for *N*-desmethyl nefopam, and 2.1 to 3.7% for nefopam *N*-oxide. The QC sample relative errors in plasma and urine ranged from −2.0% to 7.0% for nefopam, −2.0% to 11.2% for *N*-desmethyl nefopam, and −3.3% to 4.2% for nefopam *N*-oxide. Stability of nefopam, *N*-desmethyl nefopam, and nefopam *N*-oxide in heparinized human plasma was demonstrated when stored for up to 83 d at −20 °C. Stability of urine samples was demonstrated up to 83 d at −20 °C and −70 °C.

Pharmacokinetic analysis

Pharmacokinetic parameters were determined for individual subjects by standard non-compartmental analysis using Phoenix WinNonlin (Version 6.3; Certara, Princeton, NJ). Apparent elimination phase rate constant (k_{el}) was estimated by linear regression of the log-linear plasma concentration–time curve. Apparent terminal half-life ($t_{1/2}$) was calculated as $0.693/k_{el}$. Area-under-the-concentration–time curve from time zero to infinity ($AUC_{0-\infty}$) was estimated as $AUC_{0-t} + C_{last}/k_{el}$, where AUC_{0-t} is the area-under-the-concentration–time curve from time zero to last measurable concentration and C_{last} is the last measurable concentration in plasma. CL/F (apparent oral clearance, calculated by dose/$AUC_{0-\infty}$), and V_d/F (apparent volume of distribution, calculated as $[CL/F)/k_{el}]$ were estimated for total radioactivity in whole blood and plasma. Pharmacokinetic parameters were estimated based on the actual dose of nefopam (72 ± 0.07 mg free base equivalent; 96 ± 0.12 μCi) administered to each subject. Additionally, total radioactivity in blood and plasma was analyzed by compartmental modeling using Phoenix WinNonlin (Certara, Princeton, NJ). Samples with radioactivity levels below the limit of quantitation (BLQ) were considered zero for the calculation of mean and SD. During non-compartmental analysis, plasma concentration values that were BLQ after time of peak concentration (T_{max}) were censored to 0.5 ng/mL.

Sample preparation for metabolite profiling and identification

To ensure that there was sufficient radioactivity for any necessary extraction and reconstitution procedures, the samples of plasma, urine, and feces were pooled and profiled for nefopam and metabolites of [^{14}C]-nefopam as follows.

Plasma

Samples obtained at 1, 2, 4, 6, 9, 12, 24, and 48 h postdose were pooled by subject to generate single 0- to 48-h AUC-representative pooled samples, including between 75 and 2700 μL of each sample as determined by using a time-weighted pooling method (Hop et al., 1998). The radioactivity in each pooled sample was determined by liquid scintillation counting (LSC) and represented 100% of the radioactivity exposure in plasma for each individual. Approximately 1–2 g (three replicates for each subject) of the AUC-pooled plasma sample was transferred to centrifuge tubes, combined with 6 mL of acetonitrile:methanol (ACN:MeOH, 3:1, v:v), sonicated, vortexed, centrifuged, and the supernatants were removed. The extraction was repeated, and the respective supernatants were combined. Duplicate aliquots were analyzed by LSC to determine extraction recoveries, which ranged from 76.2 to 97.2%. The combined supernatants were evaporated to dryness and reconstituted in 500 μL RO water:ACN:MeOH (3:1:1, v:v:v). Samples were sonicated, vortex mixed, centrifuged, and duplicate aliquots were analyzed by LSC to determine reconstitution recoveries, which ranged from 98.4 to 100%. The reconstituted samples were analyzed by LC-MS/MS with fractions collected at 15-s intervals and analyzed by TopCount solid scintillation counting.

Urine

Samples collected at 0–3, 3–6, 6–9, 9–12, 12–24, 24–36, 36–48, 48–60, and 60–72 h postdose were pooled by subject and collection interval to generate 0- to 9-, 9- to 36-, and 36- to 72-h pooled samples, including 0.2–1.2% of each sample by weight (equivalent percent by pool) of each sample. The radioactivity in each pooled sample was determined by LSC and represented 97–98% of the radioactivity recovered in urine for each subject. Approximately 5 g of each pooled urine sample was evaporated to dryness and reconstituted in 500 μL of RO water. Samples were sonicated, vortex mixed, centrifuged, and duplicate aliquots were analyzed by LSC to determine reconstitution recoveries, which ranged from 79.1 to 100%. Due to low recoveries in the 9- to 36-h pooled urine

sample for one subject and the 36- to 72-h pooled urine sample for another subject, the samples were further reconstituted with an additional 500 µL of RO water as previously described. Reconstitution recoveries in duplicate samples were 74.5 and 90.5%. The reconstituted urine samples were analyzed by LC-MS with fractions collected at 15-s intervals and analyzed by TopCount solid scintillation counting.

Feces

Selected samples (representing 97–99% of the radioactivity recovered in feces) collected through 96 h postdose were analyzed individually as follows: 0–24 h (one subject), 24–48 h (seven subjects), 48–72 h (five subjects), and 72–96 h (three subjects). Aliquots of each fecal sample were combusted and analyzed by LSC to determine the concentrations of radioactivity. Approximately 2.3–2.8 g of each individual fecal sample was combined with 6 mL of ACN:MeOH (4:1, v:v), sonicated, vortex mixed, centrifuged, and the supernatants were removed. The extraction was repeated and the respective supernatants were combined. Extraction recoveries ranged from 72.9 to 99.4%. The combined supernatants were evaporated to dryness and reconstituted in 500 µL methanol. These samples were then sonicated, vortex mixed, centrifuged, and duplicate aliquots were analyzed by LSC to determine reconstitution recoveries, which ranged from 94.1 to 100%. The reconstituted fecal samples were analyzed by LC-MS/MS with fractions collected at 15-s intervals and analyzed by TopCount solid scintillation counting (PerkinElmer, Boston, MA).

Quantitation of metabolites

The metabolites of nefopam present in plasma, urine, and feces were quantitated based on the profiles of radioactivity. For excreta, the percentage of the administered dose excreted as the component represented by the radioactive peak was then calculated by using the following equation:

$$\% \text{ of dose} = (\% \text{ of radioactivity in peak}/100) \times \% \text{ of dose in sample}$$

The metabolite profiles in plasma extracts are reported as percentages of the total sample radioactivity, and also as concentrations (ng equivalents/g). The percent of dose and concentration in the peak was corrected for extraction and reconstitution recoveries, as applicable. For the determination of exposure to major metabolites in plasma, the total radioactivity in the HPLC run (sum of % total for all individual peaks detected) was considered to be the total radioactivity exposure in plasma from 0- to 48 h postdose, and the percent of radioactivity that each peak represented in the HPLC run was considered as the percent exposure of that metabolite (or unchanged parent) from 0- to 48 h postdose. Structures of the metabolites were identified by liquid chromatography mass spectrometry (LC-MS and/or LC-MS/MS) and were verified with reference standards, when available. In instances where the mass spectrometric fragmentation data did not adequately support definitive structural assignments, a conservative structure was presented (showing the type of biotransformation).

LC/MS procedures for metabolite identification

The HPLC system consisted of an Agilent-1200 solvent pump (Agilent Technologies, Santa Clara, CA), an Agilent-1200 membrane degasser, an Agilent-1200 autoinjector, a Perkin-Elmer 610TR radiodetector (PerkinElmer, Boston, MA), and a Leap PAL HTC-xt fraction collector (CTC Analytics AG, Zwingen, Switzerland). Chromatographic separations were performed with a Waters XSelect 3.5 µm (4.6 × 250 mm) column (Waters Corporation, Milford, MA) coupled with a C18 4 × 3 guard column (Phenomenex, Torrance, CA). The mobile phase consisted of 0.1% formic acid in RO water (solvent A) and acetonitrile (solvent B). The mobile phase gradient was as follows: flow initiated with 95% A, decreased to 82% A over 8 min, changed to 60% over 56 min, followed by a short gradient to 5% A from 64 to 70 min, and returned to initial gradient of 95% A from 73.5 to 80 min. The system was equilibrated for 3 min prior to the next injection. A flow rate of 1.0 mL/min was maintained throughout the analysis. Mass spectrometric analysis was conducted with an Agilent-6530 Q-TOF (Agilent Technologies, Santa Clara, CA) operated with dual electrospray ionization (ESI) sources. The effluent from the HPLC column was split at a 20:80 ratio to mass spectrometer:radiodetector/fraction collector/waste. The response of the radiodetector was recorded in real time by the mass spectrometer that provided simultaneous detection of radioactivity and mass spectrometry data. The mass spectrometer was operated in the positive ESI mode (4500 V) with a capillary temperature set at 325 °C.

Results

The median age of the subjects was 34.0 years (range: 27–49 years), the median body weight was 82.3 kg (range: 73.0–102.4 kg), and the body mass index was 18.0–29.5 kg/m^2. All subjects were Caucasian.

Clinical safety and tolerability

All eight subjects completed the study as planned and received treatment in the fasting state. The treatment was well tolerated with no deaths, serious adverse events, or withdrawals due to adverse events (AEs). Five subjects (63%) reported at least one AEs (scleral hyperemia, paresthesia, euphoric mood, nausea, and diarrhea), three (38%) of whom experienced at least one AE that was deemed related or possibly related to the drug. All AEs were mild-to-moderate in severity and resolved during the study without treatment or intervention.

Radioactivity in whole blood and plasma

Concentrations of total radioactivity in whole blood and plasma versus time are presented graphically in Figure 2(A). Maximum mean concentrations of drug-derived radioactivity in whole blood and plasma were observed at 2 h postdose, with values of 364 ± 31.5 and 641 ± 59.5 ng Eq free base/g, respectively. Maximum radioactivity concentrations in whole blood of individual subjects were observed from 1 to 3 h postdose and ranged from 323 to 406 ng Eq free base/g. Maximum plasma radioactivity concentrations in individual subjects were observed from

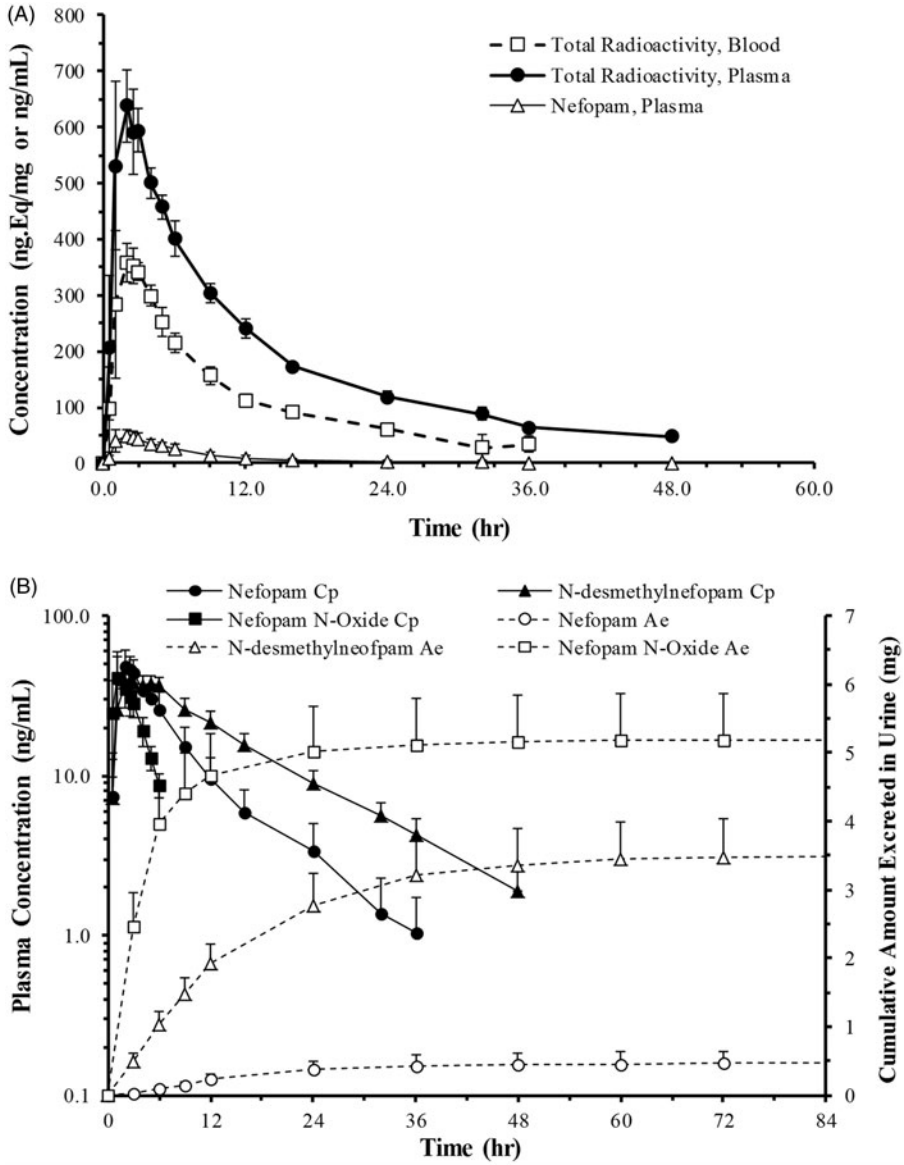

Figure 2. Mean (± SD) concentrations of (A) total radioactivity in blood and plasma, and (B) plasma concentrations (C_p) and cumulative amounts (A_e) excreted in urine for nefopam, *N*-desmethyl nefopam, and nefopam *N*-oxide in healthy male volunteers ($n = 8$) after a single oral dose of [^{14}C]-nefopam HCl (75 mg, 100 μCi). Inset shows the plasma concentration–time profiles of the analytes on an expanded scale (0–10 h). Kinetics was determined over the entire duration of study but abscissa in figure 2B is truncated at 84 hours.

2 to 3 h postdose and ranged from 543 to 711 ng Eq free base/g. Radioactivities in whole blood and plasma were BLQ in all subjects by 36 h and 48 h postdose, respectively. The mean V_d/F for total radioactivity in plasma was 165.9 L and the mean CL/F was 7.51 L/h. Blood to plasma ratio based on the mean $AUC_{0-\infty}$ was 0.53. Total radioactivity concentration–time curves in whole blood and plasma were best described by a two-compartment model with first-order absorption, k_a, of 0.42 h^{-1} or a half-life for absorption of 1.7 h. The mean percentage of radioactivity associated with red blood cells (RBC) ranged from 0.00 to 11.1% through 36 h postdose. These data indicate no noteworthy binding of radioactivity (nefopam and its metabolites) to blood cell constituents.

Pharmacokinetics of nefopam and total radioactivity in blood and plasma

The mean concentration versus time profile of nefopam compared with the total radioactivity in blood and plasma after oral administration of [^{14}C]-nefopam is presented graphically in Figure 2(A), with the associated PK parameters presented in Table 1. After a single 75 mg oral dose, concentrations of nefopam in plasma peaked in parallel to total radioactivity at approximately 2 h. Mean (± SD) terminal $t_{1/2}$ of nefopam in plasma was approximately 8.1 ± 3.6 h (Table 1) and indicates faster elimination than for total radioactivity (Table 1). The ratios of mean C_{max} and AUC_{0-t} values of nefopam and total radioactivity were 0.08 and 0.05, respectively, suggesting that intact nefopam represented a very small fraction of the total circulating radioactivity. The variability in C_{max} and AUC_{0-t} of nefopam in plasma, based on the percent coefficient of variation (% CV), was higher than of total radioactivity, ranging from 22% to 31%.

Pharmacokinetics of nefopam, *N*-desmethyl nefopam, and nefopam *N*-oxide in plasma

Mean concentration versus time profiles of nefopam, *N*-desmethyl nefopam, and nefopam *N*-oxide determined in

Table 1. Pharmacokinetic parameters of nefopam and total radioactivity in blood and plasma following a single oral dose of [^{14}C]-nefopam HCl (75 mg, 100 μCi).

Parameter[a]	Nefopam	Blood	Plasma
T_{max} (h)	2.00 (1.00–3.00)	2.00 (1.00–3.00)	2.00 (2.00–3.00)
C_{max} (ng Eq/g or ng/mL)	50.89 ± 11.25	364.4 ± 31.5	641.4 ± 59.5
AUC_{0-t} (ng Eq.h/g or ng.h/mL	394.79 ± 121.88	4137.6 ± 251.7	8546.7 ± 354.1
$AUC_{0-\infty}$ (ng Eq.h/g or ng.h/mL)	410.45 ± 122.16	5056.2 ± 198.4	9613.3 ± 527.8
$t_{1/2}$ (h)	8.08 ± 3.06	15.3 ± 1.40	15.4 ± 2.33
V_d/F (L)	NA	314.0 ± 31.1	165.9 ± 21.7
CL/F (L/h)	NA	14.3 ± 0.55	7.51 ± 0.41

[a]Mean (SD) values shown for C_{max}, $t_{1/2}$, and AUC ($n = 8$); median (range) noted for T_{max}.

Table 2. Pharmacokinetic parameters of *N*-desmethyl nefopam, and nefopam *N*-oxide in plasma following a single oral dose of [^{14}C]-nefopam HCl (75 mg, 100 μCi).

Parameter[a]	*N*-desmethyl nefopam	Nefopam *N*-oxide
T_{max} (h)	2.50 (2.00–6.00)	1.00 (1.00–2.00)
C_{max} (ng/mL)	41.45 ± 5.65	42.86 ± 11.36
AUC_{0-t} (ng.h/mL)	647.49 ± 79.36	142.93 ± 35.34
$AUC_{0-\infty}$ (ng.h/mL)	672.93 ± 83.82	164.99 ± 38.33
$t_{1/2}$ (h)	10.25 ± 1.38	1.77 ± 0.17

[a]Mean (SD) values shown for C_{max}, $t_{1/2}$, and AUC ($n = 8$); median (range) noted for T_{max}.

plasma by the validated LC-MS/MS method after oral administration of [^{14}C]-nefopam are presented graphically in Figure 2(B), with the associated PK parameters in Table 2. Plasma concentrations of nefopam, *N*-desmethyl nefopam, and nefopam *N*-oxide peaked at approximately 2.0, 2.5, and 1.0 h, respectively. C_{max} of all three analytes were comparable. Total exposure (assessed by AUC values) of *N*-desmethyl nefopam was highest followed by nefopam and the *N*-oxide metabolite. *N*-desmethyl nefopam, and nefopam were quantifiable in plasma for up to 32 and 48 h postdose, whereas nefopam *N*-oxide levels were BLQ after 12 h (LLOQ for the *N*-oxide was higher). Apparent terminal $t_{1/2}$ values for nefopam, *N*-desmethyl nefopam, and nefopam *N*-oxide were 8.1, 10.2, and 1.8 h, respectively (Table 2). The ratios of mean C_{max} and mean AUC_{0-t} of *N*-desmethyl nefopam to total radioactivity in plasma were 0.06 and 0.08, respectively, suggesting that *N*-desmethyl nefopam accounted for less than 8% of circulating radioactivity. The ratios of mean C_{max} and mean AUC_{0-t} of nefopam *N*-oxide to total radioactivity in plasma were 0.06 and 0.02, respectively, suggesting that the *N*-oxide accounted for $<2\%$ of the circulating radioactivity.

Mass balance and excretion in urine and feces

The mean cumulative percentages of radioactive dose recovered in urine and feces are presented in Figure 3. The mean ± SD of total recovery of radioactivity in urine and feces over the 168-h assessment period was approximately 92.6 ± 3.22%, with recoveries in individual subjects ranging from 87.9 to 97.5%. Most of the administered radioactivity (83.1%) was excreted in the first 48 h postdose. A majority of the [^{14}C]-nefopam dose was excreted in urine (79.3 ± 3.60%) with a smaller amount excreted in feces (13.4 ± 0.55%). The excretion of radioactivity in urine was rapid; the mean cumulative recovery at 24 h was 66.9 ± 4.29% which accounted for greater than 80% of total radioactivity

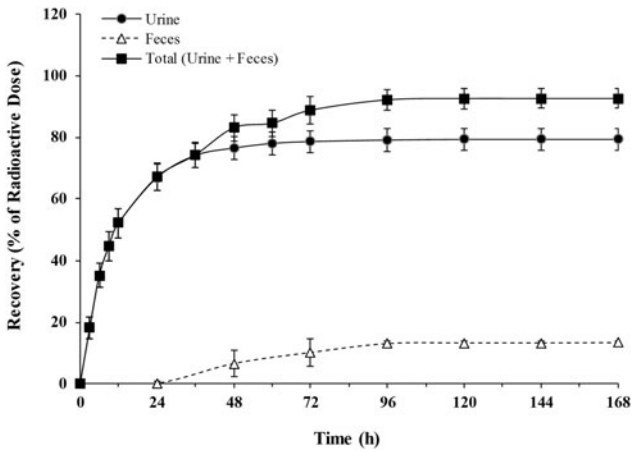

Figure 3. Mean ± SD cumulative percent of radioactive dose recovered in urine, feces, and sum of urine and feces at specified intervals after a single oral dose of [^{14}C]-nefopam HCl (75 mg, 100 μCi) to healthy male subjects ($n = 8$).

recovered in urine. Urinary excretion of radioactivity appeared to plateau after 2 d in all subjects whereas radioactivity continued to be excreted in feces for up to 4 d.

Metabolite profiles in biological matrices

Due to low radioactivity levels in the samples, plasma and urine were pooled (as applicable) to ensure that there was sufficient radioactivity for extraction and reconstitution procedures. This strategy precluded the determination of time course of various metabolites.

Plasma

A representative radio-HPLC chromatogram from reconstituted plasma extracts is presented in Figure 4(A). Quantification of [^{14}C]-nefopam and its metabolites in plasma (0- to 48-h) of individual subjects based on radio-HPLC is presented in Table 3. The mean sample recovery of radioactivity in pooled plasma extracts used for metabolite profiling was 95.3 ± 3.95% (Table 3) suggesting that radioactivity was not covalently bound to plasma proteins. Radio HPLC profiles obtained from analysis of plasma extracts from all subjects were generally qualitatively similar and showed up to 12 radioactive peaks. Unchanged [^{14}C]-nefopam was a minor component in plasma representing 4.53 ± 2.45%, of the total radioactivity exposure. The radioactive exposure in plasma was mostly related to metabolites of [^{14}C]-nefopam. The major metabolites detected (representing a mean of greater than 10% of the radioactivity in plasma) were

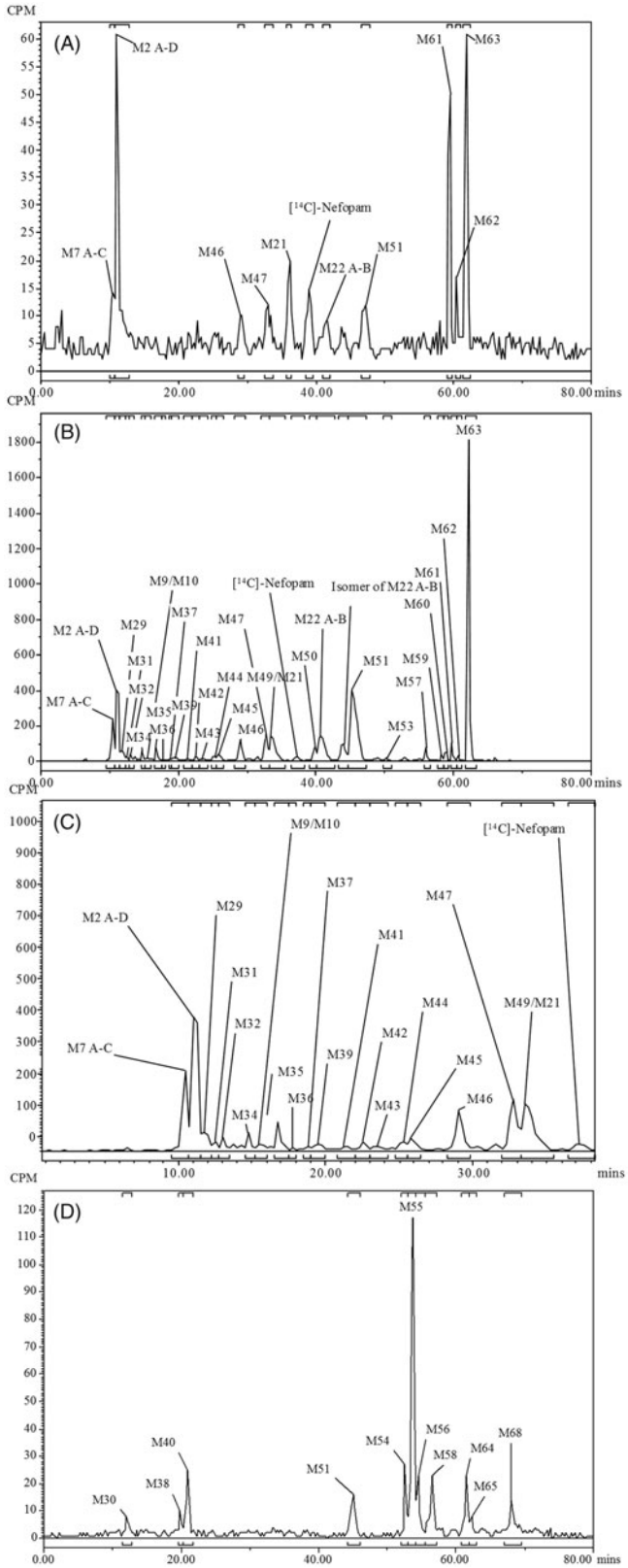

Figure 4. Representative radiochromatogram of (A) a 0- to 48-h AUC-pooled plasma sample, (B) a 0- to 9-h pooled urine sample, (C) the 0- to 9-h pooled urine sample shown in an expanded scale, and (D) a 24- to 48-h fecal sample obtained from one of the eight subjects after a single oral dose of [^{14}C]-nefopam HCl (75 mg, 100 μCi). The pooled plasma sample was from Subject 110-003, urine sample was from Subject 110-001, and feces sample was from Subject 110-002. The limit of quantitation for plasma was set at 1% of run or 10 cpm peak height.

metabolites M2 A-D (*N*-demethylation coupled with oxidation and glucuronidation), M61 (*N*-demethylation coupled with glucose conjugation, dehydration, and glucuronidation), and M63 (*N*-demethylation coupled with *N*-glucuronidation) representing $16.7 \pm 5.74\%$, $29.5 \pm 9.21\%$, and $26.6 \pm 2.51\%$ (mean ± SD) of the total radioactivity exposure in plasma from 0- to 48-h postdose, respectively. Minor metabolites detected (representing a mean of greater than 2% of the radioactivity in plasma) were M47 (*N*-glucuronidation), M21 (*N*-desmethyl nefopam), M22 A-B ((1R,5R)(1S,5S)-Nefopam *N*-oxide), M51 (*N*-demethylation coupled with ring opening and carboxylic acid formation, or di-oxidation), and M62 (*N*-demethylation coupled with glucose conjugation and dehydration), representing $3.31 \pm 3.41\%$, $5.03 \pm 3.96\%$, $2.07 \pm 2.02\%$, $2.26 \pm 1.97\%$, and $2.73 \pm 0.928\%$ (mean ± SD) of the total radioactivity in plasma from 0- to 48-h postdose, respectively. Metabolites M7 A-C (di-oxidation coupled with hydrogenation and glucuronidation), M29 (mono-oxidation coupled with glucuronidation), and M46 (*N*-glucuronidation) each represented (where detected) a mean of less than 2% of the total radioactivity exposure in plasma from 0- to 48-h postdose. The relatively low abundance of nefopam, *N*-desmethyl nefopam, and nefopam *N*-oxide in plasma is consistent with the results of bioanalysis using a validated LC-MS/MS method which indicates that the three account for a small part of the total radioactivity (approximately 5%, 8%, and 2% based on AUC).

Urine

A representative radio-HPLC chromatogram from urine constituents is presented in Figure 4(B). Quantification of [^{14}C]-nefopam and its metabolites in urine based on radio-HPLC is presented in Table 4. Radio HPLC profiles obtained from analysis of urine reconstitutes from all subjects were qualitatively similar (data not shown) and showed up to 32 radioactive peaks. A mean (± SD) of $78.6 \pm 3.62\%$ of the total administered radioactive dose excreted in urine was pooled for profiling, of which a mean of $71.4 \pm 3.32\%$ of the dose was quantitated as unchanged [^{14}C]-nefopam and its metabolites. Unchanged [^{14}C]-nefopam in urine was present in trace amounts (a mean of $0.611 \pm 0.317\%$). The major metabolites (representing greater than 8% of the administered radioactive dose) were M2 A-D, M51, and M63, representing a mean (±SD) of $9.82 \pm 2.04\%$, $8.06 \pm 2.02\%$, and $22.9 \pm 3.96\%$ of the administered radioactive dose through 72 h postdose, respectively. Minor metabolites (representing greater than 1% but less than 8% of the administered radioactive dose) were M7 A-C, M29, M46, M47, M49 (*N*-demethylation coupled with ring opening, mono-oxidation and glucuronidation), M21, M22 A-B, isomer of M22 A-B, M60 (*N*-demethylation coupled with mono-oxidation and glucuronidation), and M61, representing a mean (± SD) of $2.81 \pm 1.16\%$, $1.44 \pm 0.518\%$, $1.80 \pm 0.481\%$, $1.72 \pm 0.524\%$, $2.90 \pm 1.43\%$, $2.47 \pm 1.09\%$, $4.38 \pm 0.501\%$, $1.67 \pm 0.283\%$, $1.14 \pm 0.434\%$, and $1.57 \pm 0.425\%$ of the administered radioactive dose through 72 h postdose, respectively. All other metabolites detected were present in trace amounts, each representing a mean of less than 1% of the administered radioactive dose through 72 h postdose.

Table 3. Percent of [^{14}C]-nefopam or its metabolites in 0- to-48 h AUC pooled plasma samples obtained from male human subjects following a single oral dose of [^{14}C]-nefopam HCl (75 mg, 100 μCi).

		Percent of radioactivity injected (% of run)									
		Subject number									
Final metabolite designation	Retention time (min)	110-001	110-002	110-003	110-004	110-005	110-006	110-007	110-008	Mean	SD
M7 A-C	10.63	1.67	ND	3.27	3.84	ND	ND	1.24	0.72	1.34	1.51
M2 A-D	11.13	15.63	9.57	24.69	20.00	20.44	19.76	7.80	15.41	16.7	5.74
M29	11.88	ND	ND	ND	3.23	ND	ND	ND	ND	0.404	1.14
M46	28.88–29.38	0.83	ND	1.51	1.21	0.89	1.80	ND	1.08	0.915	0.647
M47	32.63–33.88	3.13	1.01	3.27	1.62	2.22	2.69	1.06	11.47	3.31	3.41
M21	34.88–36.63	7.08	9.32	6.05	5.45	10.22	ND	ND	2.15	5.03	3.96
[^{14}C]-Nefopam	37.13–39.88	2.92	1.51	4.79	2.22	8.00	8.08	4.79	3.94	4.53	2.45
M22 A-B	39.63–41.63	2.08	1.76	1.26	ND	1.33	4.49	5.67	ND	2.07	2.02
M51	45.63–47.88	3.96	3.53	4.03	ND	2.22	ND	ND	4.30	2.26	1.97
M61	59.38–60.13	15.83	40.55	18.89	31.72	28.44	31.44	42.02	27.24	29.5	9.21
M62	60.63–61.13	2.50	4.03	2.52	2.83	1.33	2.40	4.08	2.15	2.73	0.928
M63	61.88–62.38	30.42	25.44	25.44	23.64	24.44	25.45	29.79	27.96	26.6	2.51
Total		86.1	96.7	95.7	95.8	99.5	96.1	96.5	96.4	95.3	3.95

ND, peak not detected; SD, standard deviation.

Feces

A representative radio-HPLC chromatogram from feces reconstitutes is presented in Figure 4(C). Quantification of [^{14}C]-nefopam and its metabolites in feces based on radio-HPLC is presented in Table 4. Radio HPLC profiles obtained from analysis of fecal extracts from all subjects were generally qualitatively similar (data not shown) and showed up to 19 radioactive peaks. A mean of $12.7 \pm 0.779\%$ of the total administered radioactive dose excreted in feces was pooled for profiling, of which a mean ($\pm$ SD) of $9.99 \pm 0.448\%$ of the dose was quantitated as nefopam metabolites. Unchanged nefopam was not detected in fecal extracts, suggesting that [^{14}C]-nefopam was completely absorbed or that any unabsorbed [^{14}C]-nefopam was degraded in the GI tract to other components. The major metabolite detected in the fecal extracts was M55 (unknown), representing a mean of $4.63 \pm 0.468\%$ of the administered radioactive dose in feces through 96 h postdose, as applicable. Minor metabolites detected in the fecal extracts were M40 (unknown) and M51 (ring opening and carboxylic acid formation (or) di-oxidation), representing a mean ($\pm$ SD) of 0.900 ± 0.121 and $0.947 \pm 0.219\%$ of the administered radioactive dose in feces through 96 h postdose. All the remaining metabolites detected in fecal extracts were present in trace amounts, each representing a mean of less than 0.9% of the administered radioactive dose through 96 h postdose. The presence of metabolites in fecal extracts suggests hepatobiliary excretion of [^{14}C]-nefopam-related radioactivity, other non-biliary route(s) of excretion of drug-related radioactivity from systemic circulation into the gastrointestinal tract, or metabolism within the GI tract.

Structural elucidation of major metabolites

Using LC-MS and LC-MS/MS techniques, parent and 31 metabolites were detected and identified (data not shown) in human plasma, urine, and fecal samples. Representative product ion mass spectra and the fragment assignments for

Table 4. Mean total percent of radioactive dose as [^{14}C]-nefopam or its metabolites in pooled urine and feces samples obtained from male human subjects following a single oral dose of [^{14}C]-nefopam HCl (75 mg, 100 μCi).

	Percent of radioactive dose			
	Urine		Feces	
Metabolite designation	Mean	SD	Mean	SD
M7 A-C	2.81	1.16	ND	NA
M2 A-D	9.82	2.04	0.0903	0.0791
M29	1.44	0.518	ND	NA
M30	ND	NA	0.284	0.0809
M31	0.866	0.589	ND	NA
M32	0.75	0.176	ND	NA
M34	0.595	0.289	ND	NA
M9/M10	0.535	0.239	ND	NA
M35	0.653	0.134	ND	NA
M36	0.205	0.0767	ND	NA
M39	0.396	0.178	ND	NA
M41	0.184	0.079	ND	NA
M42	0.395	0.0759	ND	NA
M43	0.388	0.172	ND	NA
M44	0.429	0.11	ND	NA
M45	0.538	0.243	ND	NA
M46	1.8	0.481	ND	NA
M47	1.72	0.524	ND	NA
M49	2.9	1.43	ND	NA
M21 (*N*-desmethyl nefopam)	2.47	1.09	ND	NA
[^{14}C]-Nefopam	0.611	0.317	ND	NA
M50	0.762	0.238	ND	NA
[a]M22 A-B (nefopam *N*-oxide)	4.38	0.501	ND	NA
[a]M22 A-B (isomer)	1.67	0.283	ND	NA
M51	8.06	2.02	0.947	0.219
M53	0.251	0.0852	ND	NA
M57	0.647	0.128	ND	NA
M59	0.332	0.136	ND	NA
M60	1.14	0.434	ND	NA
M61	1.57	0.425	ND	NA
M62	0.444	0.0948	ND	NA
M63	22.9	3.96	ND	NA
Total percent of dose identified	71.66	NA	1.3	NA

ND, not detected; NA, not applicable; SD, standard deviation.
[a]Metabolites co-eluted in HPLC analysis.

nefopam, *N*-desmethyl nefopam, and nefopam *N*-oxide standards are presented in Figure 5(A–C), respectively. Selected mass spectra data for nefopam and its metabolites; and the biotransformations are presented in Table 5. The elemental composition of nefopam and its metabolites listed in Table 6 were confirmed using accurate mass analysis. The basis for the mass-spectral identification of the metabolites of nefopam was through the knowledge of the fragmentation routes of nefopam itself. Previously known or suspected metabolites of nefopam (*N*-desmethyl nefopam and nefopam *N*-oxide) are highlighted in bold (Table 5).

Nefopam

The mass spectrum showed the protonated molecular ion at *m/z* 254 consistent with the mass of nefopam, and product ions at *m/z* 181, 179, 166, and 72. The elemental composition of nefopam in both the mixed standard solution and study samples was confirmed using accurate mass analyses (Table 5).

N-desmethyl nefopam (M21)

The mass spectrum showed the protonated molecular ion at *m/z* 240 consistent with the mass of *N*-desmethyl nefopam, and product ions at *m/z* 181, 179, 166, 118, and 91. The elemental composition of *N*-desmethyl nefopam in both the mixed standard solution and study samples was confirmed using accurate mass analyses (Table 5).

Nefopam N-oxide (M22A-B)

The mass spectrum showed the protonated molecular ion at *m/z* 270 consistent with the mass of nefopam *N*-oxide, and product ions at *m/z* 195, 181, 179, 74, and 56. The elemental composition of nefopam *N*-oxide in both the mixed standard solution and study samples was confirmed using accurate mass analyses (Table 5).

Metabolite M2 A-D (isomeric mixtures)

A representative product ion mass spectrum of metabolite M2 A-D obtained from analysis of a study sample is shown in Figure 6(A). The protonated molecular ion of M2 was *m/z* 432, and the common product ions to nefopam were *m/z* 179 and *m/z* 166. The *m/z* of 432 suggested that nefopam underwent *N*-demethylation, coupled with oxidation and subsequent glucuronidation. The presence of the product ion at *m/z* 256 represented a neutral loss of 176 Da, which is characteristic of glucuronide conjugates. The presence of the product ion at *m/z* 256 also suggested that one oxidation and demethylation had occurred. The presence of the product ion at *m/z* 162 suggested that the oxidation had occurred on the terminal phenyl ring. The exact positions of oxidation and conjugation could not be determined due to limited mass spectral fragmentation data. The elemental composition of metabolite M2 A-D was confirmed using accurate mass analysis (Table 5).

M61

A representative product ion mass spectrum of metabolite M61 obtained from analysis of a study sample is shown in Figure 6(B). The protonated molecular ion of M61 was *m/z* 578, and the common product ion to nefopam was *m/z* 179. The *m/z* of 578 suggested that nefopam underwent *N*-demethylation coupled with glucose conjugation, dehydration, and glucuronidation. The presence of the product ions at *m/z* 402 and 240 represents sequential neutral losses of 176 Da and 162 Da, which is characteristic of glucuronide and glucose conjugates, respectively. The exact position of the glucuronidation could not be determined from the limited mass spectral fragmentation data. The elemental composition of metabolite M61 was confirmed using accurate mass analysis (Table 5).

M63

A representative product ion mass spectrum of metabolite M63 obtained from analysis of a study sample is shown in Figure 6(C). The protonated molecular ion of M63 was *m/z* 416, and the common product ion to nefopam was *m/z* 181. The *m/z* of 416 suggested that nefopam underwent *N*-demethylation coupled with *N*-glucuronidation. The presence of the product ion at *m/z* 240 (a loss of 176 Da) as an in-source fragment and major ion in the MS/MS spectrum suggested that M63 was a glucuronide conjugate of *N*-desmethyl nefopam The elemental composition of metabolite M63 was confirmed using accurate mass analysis (Table 5).

M51

Representative product ion mass spectra of metabolite M51 obtained from analysis of a study sample are shown in Figure 6(D). The protonated molecular ion of M51 was *m/z* 286, and the common product ions to nefopam were *m/z* 181, 179, and 166. The *m/z* of 210 suggested that nefopam underwent ring opening and carboxylic acid formation (or) di-oxidation. The presence of the product ion at *m/z* 210 suggested that the two oxidations had occurred on the bridging ethyl portion of the oxazocine ring. However, the exact position of the oxidations could not be determined from the mass spectral data. The elemental composition of metabolite M51 was confirmed using accurate mass analysis (Table 5).

Proposed biotransformation pathway

[^{14}C]-nefopam was extensively metabolized via both Phase I and Phase II biotransformation pathways as evident by the number of metabolites observed and the percent of dose each metabolite comprised in excreta. Identified metabolites were products of mono- and di-oxidations, *N*-oxidations, carboxylic acid formation, glucuronidations, hydrogenation, *N*-demethylation, ring openings, sulfation, glucose conjugation, dehydration, or combinations thereof (data not shown). The major biotransformation pathways involved *N*-demethylation coupled with oxidation and glucuronidation (M2), *N*-demethylation coupled with glucose conjugation, dehydration and glucuronidation (M61), *N*-demethylation coupled with *N*-glucuronidation (M63), ring opening, and carboxylic acid formation (or) di-oxidation (M51). A biotransformation pathway for orally administered [^{14}C]-nefopam in humans is proposed in Figure 7.

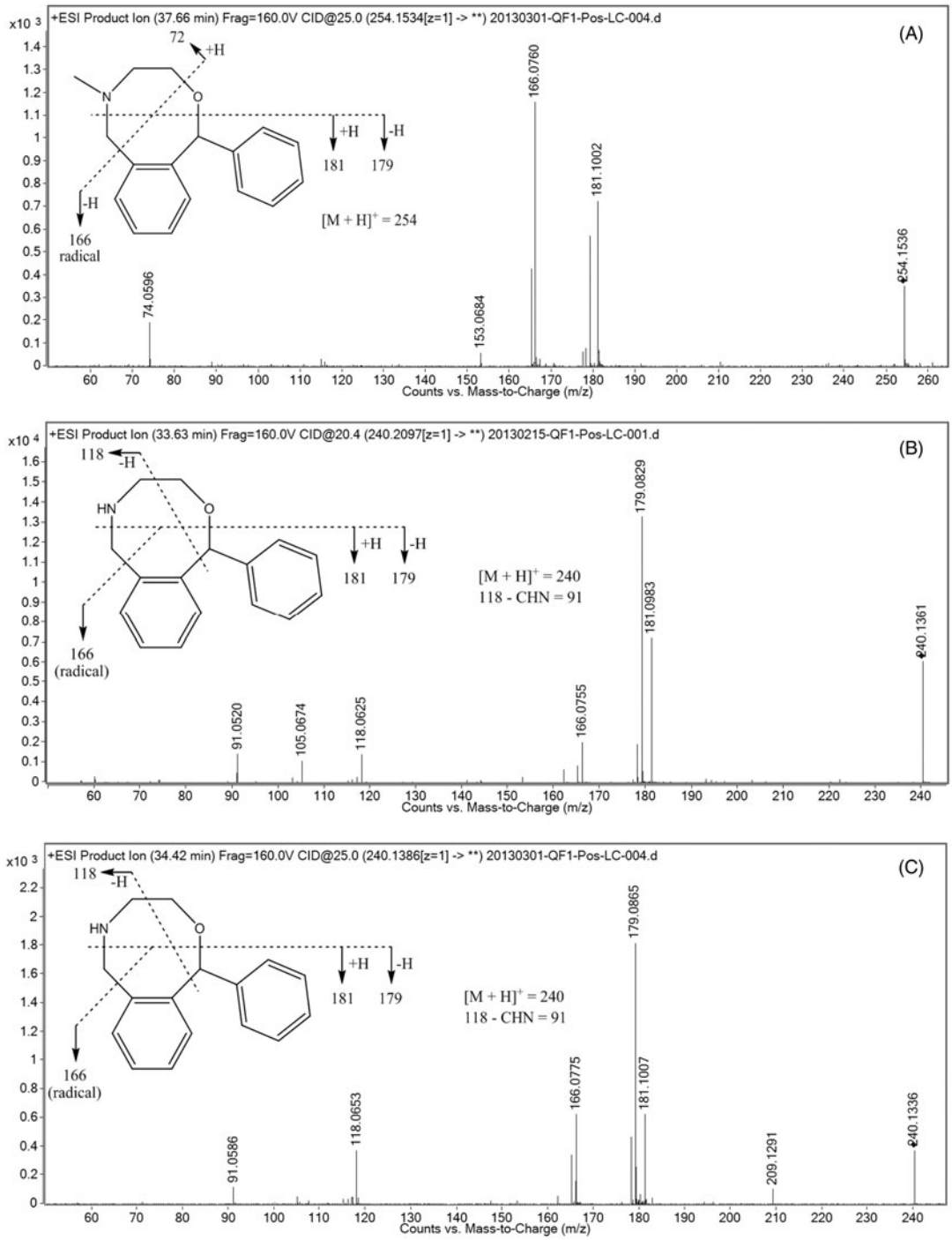

Figure 5. Product ion mass spectrum of (A) nefopam, (B) *N*-desmethyl nefopam (M21), and (C) (lR,5R)/(lS,5S)-nefopam *N*-oxide (M22 A-B) obtained from analysis of authentic standard solutions. Insets show the structures and proposed fragmentation patterns.

Discussion

In this work, we characterized the pharmacokinetics, excretion, and metabolism of nefopam after administration of a single 75 mg oral dose to humans. A radioactivity dose of 100 μCi of [^{14}C]-nefopam was administered based on radiation dosimetry estimated from a tissue distribution study of [^{14}C]-nefopam in Long–Evans pigmented rats (data on file).

The approximately two-fold higher concentration of total radioactivity in plasma than blood suggested a lack of accumulation in RBCs. Minimal association of nefopam or metabolites with RBCs was noted. Total radioactivity in blood and plasma generally mirrored each other including T_{max} and $t_{1/2}$. The mean V_d/F of 165.9 L and a mean CL/F of 7.51 L/h for total radioactivity in plasma suggested that radioactivity derived from nefopam is well distributed to tissues. Circulating concentrations of nefopam in plasma reached a peak at about the same time as total radioactivity. Mass balance was demonstrated with a mean total radioactivity recovery of 93% by day 7. Approximately, 73% and

Table 5. Summary of characteristic product ions and biotransformation pathways for nefopam and its identified metabolites in biological matrices.

Final designation	[M + H]+	Characteristic product ions (*m/z*)	*m/z* Shift from Parent	Proposed biotransformation	Matrix
Nefopam	254	181, 179, 166, 74	–	Nefopam	Plasma, urine
M7 A-C	464	288, 167	210	Di-oxidation coupled with hydrogenation and glucuronidation	Plasma, urine
M2 A-D	432	256, 162	178	*N*-Demethylation coupled with oxidation and glucuronidation	Plasma, urine
M29	446	270	192	Mono-oxidation coupled with glucuronidation	Plasma, urine
M30	272	162, 118	192	*N*-Demethylation coupled with di-oxidation	Feces
M31	446	270	18	Mono-oxidation coupled with glucuronidation	Urine
M32	366	286, 225, 162	112	Di-oxidation coupled with sulfation	Urine
M34	446	270, 234	192	Mono-oxidation coupled with *N*-glucuronidation	Urine
M9/M10	256	162, 118	2	*N*-Demethylation coupled with mono-oxidation	Urine
M35	446	270	192	Mono-oxidation coupled with glucuronidation	Urine
M36	256	167, 60	2	*N*-Demethylation coupled with mono-oxidation	Urine
M39	256	167, 60	2	*N*-Demethylation coupled with mono-oxidation	Urine
M41	434	240, 197, 179	180	*N*-Demethylation coupled with mono-oxidation, hydrogenation, and glucuronidation	Urine
M42	448	197, 179	194	Ring opening coupled with mono-oxidation and glucuronidation	Urine
M43	434	197, 179	180	*N*-Demethylation coupled with mono-oxidation, hydrogenation, and glucuronidation	Urine
M44	448	179, 113	194	Ring opening coupled with mono-oxidation and glucuronidation	Urine
M45	430	254, 234	176	*N*-Glucuronidation	Plasma, urine
M46	430	254, 234	176	*N*-Glucuronidation	Plasma, urine
M47	430	254, 234	176	*N*-Glucuronidation	Plasma, urine
M49	434	196	180	*N*-Demethylation coupled with ring opening, mono-oxidation, and glucuronidation	Urine
M21	240	181, 179, 166, 118, 91	−14	*N*-Desmethyl-nefopam	Plasma, urine, feces
M50	272	196, 179	18	*N*-Demethylation coupled with di-oxidation	Urine
M22 A-B	270	195, 181, 179, 74, 56	16	(1R,5R)(1S,5S)-Nefopam *N*-oxide	Plasma, urine
M22 A-B (isomer)	270	195, 181, 179, 74, 56	16	Isomer of (1R,5R)(1S,5S)-Nefopam *N*-Oxide	Plasma, urine
M51	286	210	32	Ring opening and carboxylic acid formation (or) di-oxidation	Plasma, urine, feces
M53	464	288	210	Di-oxidation coupled with hydrogenation and glucuronidation	Plasma, urine
M57	432	256, 73, 60	178	*N*-Demethylation coupled with mono-oxidation and glucuronidation	Urine
M59	432	256, 208	178	*N*-Demethylation coupled with mono-oxidation and glucuronidation	Urine
M60	432	256, 208	178	*N*-Demethylation coupled with mono-oxidation and glucuronidation	Urine
M61	578	402, 240	324	*N*-Demethylation coupled with glucose conjugation, dehydration, and glucuronidation	Plasma, urine
M62	402	240	148	*N*-Demethylation coupled with glucose conjugation and dehydration	Plasma, urine
M63	416	240	162	*N*-Demethylation coupled with *N*-glucuronidation	Plasma, urine

27% of the total administered radioactive dose was recovered in urine and feces, respectively, indicating that at least 73% of the drug was orally absorbed. These results are generally consistent with the mass balance, metabolism, and excretion pattern of [^{14}C]-nefopam in non-clinical species (data on file).

Of the total radioactivity excreted in human excreta, unchanged nefopam constituted trace amounts of the dose suggesting that nefopam was completely absorbed and extensively metabolized and subsequently excreted in urine, or that any unabsorbed nefopam was degraded in the GI tract to other components. Peak plasma concentrations of nefopam, *N*-desmethyl nefopam, and nefopam *N*-oxide were comparable but the latter peaked earlier suggesting that some or all the *N*-oxide was formed in the gastrointestinal tract. *N*-desmethyl nefopam was approximately two-fold more abundant in plasma than nefopam and five-fold more than the *N*-oxide. The mean combined AUCs of nefopam, *N*-desmethyl nefopam, and nefopam *N*-oxide accounted for approximately 14% of the total radiocarbon in circulation, whereas combined AUCs of nefopam, *N*-desmethyl nefopam, and nefopam *N*-oxide in individual subjects ranged from 9 to 18%. The apparent terminal $t_{1/2}$ values of nefopam, *N*-desmethyl nefopam, and nefopam *N*-oxide were all shorter than that of total radioactivity. The terminal $t_{1/2}$ of total radioactivity reflects the composite half-life of nefopam and all its metabolites and, therefore, represents a mixture of compounds with potentially widely varying half-lives. The longer terminal $t_{1/2}$ of total radioactivity likely reflects the presence of one or more metabolites with a longer half-life than that of nefopam, *N*-desmethyl nefopam, and the *N*-oxide. Variability is not a plausible explanation for the difference between half-lives of total radioactivity and the three known metabolites since the PK parameter estimates in this study and their variability (%CV) are consistent with that reported in the

Table 6. Summary of protonated molecular ions and representative accurate mass data for nefopam and its identified metabolites.

Final metabolite designation	$[M+H]^+$	Measured mass	Theoretical mass	Proposed formula	Δ m*D*a	Δ ppm
M7 A-C	464	464.1931	464.1915	$C_{23}H_{30}NO_9^+$	1.60	3.4
M2 A-D	432	432.1656	432.1653	$C_{22}H_{26}NO_8^+$	0.30	0.7
M29	446	446.1815	446.1809	$C_{23}H_{28}NO_8^+$	0.60	1.3
M31	272	446.1816	446.1809	$C_{23}H_{28}NO_8^+$	0.70	1.6
M30	446	272.1286	272.1281	$C_{16}H_{18}NO_3^+$	0.50	1.8
M32	366	366.1004	366.1006	$C_{17}H_{20}NSO_6^+$	−0.20	−0.5
M34	446	446.1810	446.1809	$C_{23}H_{28}NO_8^+$	0.10	0.2
M9/M10	256	256.1330	256.1332	$C_{16}H_{18}NO_2^+$	−0.20	−0.8
M35	446	446.1823	446.1809	$C_{23}H_{28}NO_8^+$	1.40	3.1
M36	256	256.1329	256.1332	$C_{16}H_{18}NO_2^+$	−0.30	−1.2
M39	256	256.1333	256.1332	$C_{16}H_{18}NO_2^+$	0.10	0.4
M41	434	434.1814	434.1809	$C_{22}H_{28}NO_8^+$	0.50	1.2
M42	448	448.1968	448.1966	$C_{23}H_{30}NO_8^+$	0.20	0.4
M43	434	434.1817	434.1809	$C_{22}H_{28}NO_8^+$	0.80	1.8
M44	448	448.1967	448.1966	$C_{23}H_{30}NO_8^+$	0.10	0.2
M45	430	430.1860	430.1860	$C_{23}H_{28}NO_7^+$	0.00	0.0
M46	430	430.1863	430.1860	$C_{23}H_{28}NO_7^+$	0.30	0.7
M47	430	430.1863	430.1860	$C_{23}H_{28}NO_7^+$	0.30	0.7
M49	434	434.1815	434.1809	$C_{22}H_{28}NO_8^+$	0.60	1.4
M21	240	240.1383	240.1383	$C_{16}H_{18}NO^+$	0.00	0.0
Nefopam	254	254.1536	254.1539	$C_{17}H_{20}NO^+$	−0.30	−1.2
M50	272	272.1282	272.1281	$C_{16}H_{18}NO_3^+$	0.10	0.4
M22 A-B	270	270.1487	270.1489	$C_{17}H_{20}NO_2^+$	−0.20	−0.7
M22 A-B (isomer)	270	270.1486	270.1489	$C_{17}H_{20}NO_2^+$	−0.30	−1.1
M51	286	286.1437	286.1438	$C_{17}H_{20}NO_3^+$	−0.10	−0.3
M53	464	464.1906	464.1915	$C_{23}H_{30}NO_9^+$	−0.90	−1.9
M57	432	432.1659	432.1653	$C_{22}H_{26}NO_8^+$	0.60	1.4
M59	432	432.1640	432.1653	$C_{22}H_{26}NO_8^+$	−1.30	−3.0
M60	432	432.1655	432.1653	$C_{22}H_{26}NO_8^+$	0.20	0.5
M61	578	578.2229	578.2232	$C_{28}H_{36}NO_{12}^+$	−0.30	−0.5
M62	402	402.1925	402.1911	$C_{22}H_{28}NO_6^+$	1.40	3.5
M63	416	416.1706	416.1704	$C_{22}H_{26}NO_7^+$	0.20	0.5

Values are representative unless otherwise noted. Δ mDa = (measured mass – theoretical mass) * 1000.
Δ ppm = (Δ mDa/theoretical mass) * 1000.

literature. *N*-desmethyl nefopam was cleared from plasma with a $t_{1/2}$ value that was similar or slightly longer than nefopam. Plasma concentrations of nefopam *N*-oxide declined faster than nefopam raising the possibility that the *N*-oxide is generated by intestinal metabolism during absorption. Estimating the true elimination rate of nefopam *N*-oxide will require it to be administered directly along with an assay of higher sensitivity.

A total of 31 metabolites were identified in human plasma and excreta by LC-MS/MS (Table 4). The primary biotransformation pathway involved *N*-demethylation coupled with oxidation and glucuronidation (M2), *N*-demethylation coupled with glucose conjugation, dehydration and glucuronidation (M61), *N*-demethylation coupled with *N*-glucuronidation (M63), ring opening, and carboxylic acid formation (or) di-oxidation (M51). The metabolites M63 and M2 A-D were present at high levels in both plasma and urine, whereas an unknown metabolite M55 was the major form excreted in feces. *N*-Desmethyl nefopam and nefopam *N*-oxide were present at low levels as also confirmed by the validated LC-MS/MS method.

The relative abundance of the hitherto unreported metabolites M2, M51, M61, and M63 in the circulation and in urine is new findings that warrant analysis in future studies. Our strategy to pool plasma and urine samples precluded us from determining the concentration–time profiles of these major metabolites. The biological activity of these new metabolites is unknown. Conjugation with glutathione, glucuronic acid, and sulfuric acid are not known to result in active metabolites with the exception of morphine-6-glucuronide and 4-hydroxytriamterene sulfate (Mulder, 1992). To better estimate the contribution of metabolites M2, M61, and M63 to the *in vivo* pharmacological effects of nefopam, their intrinsic potency and protein binding characteristics will have to be determined. Broad receptor profiling and affinity assessments of *N*-desmethyl nefopam and the diastereomers of nefopam *N*-oxide [(1R,5R)/(1S,5S), 1R,5S)/(1S,5R)] competitive radioligand binding assays show that their pharmacological profiles mirror that of nefopam albeit at higher concentrations (unpublished results, Impax).

A comparison of the metabolic profile of nefopam in the circulation and excreta of humans and rats did not reveal any human-specific metabolites (data on file, Impax). All the major identified human metabolites were present in the rat, a species used for long-term safety and toxicology assessments. However, some differences were noted with respect to the relative abundance of individual metabolites formed in each species.

In summary, this mass balance study in healthy volunteers demonstrated that orally administered nefopam is well absorbed and highly metabolized to numerous metabolites. Intact nefopam was a minor component of total radioactivity in the circulation; and renal and fecal excretion of unchanged nefopam was negligible.

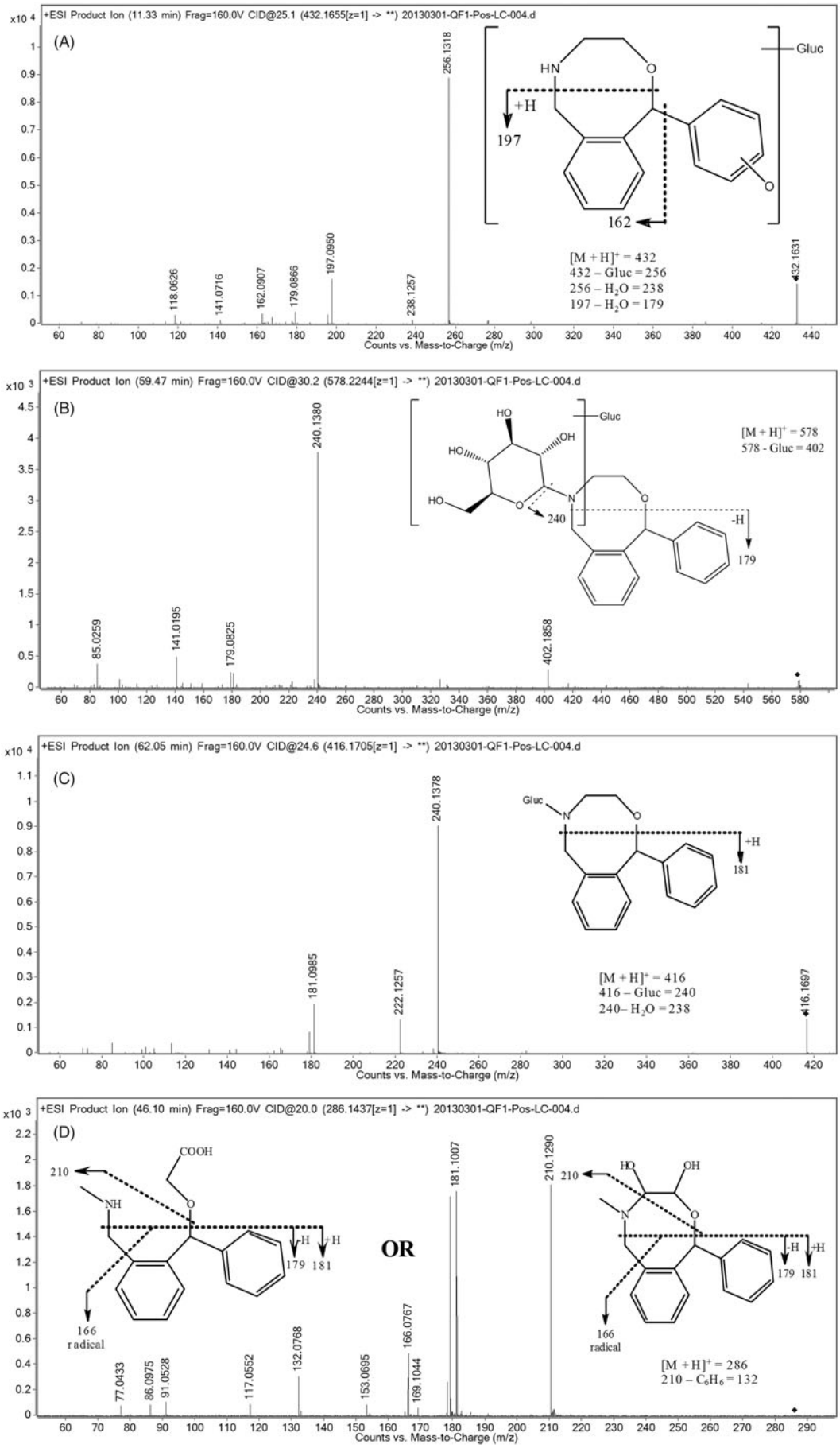

Figure 6. Product ion mass spectrum of metabolites (A) M2 (A-D), (B) M61, (C) M63, and (D) M51 obtained from analysis of a 9-to 36- h urine sample collected from human male Subject no. 110-008 after a single oral administration of [^{14}C]-nefopam HCl (75 mg, 100 μCi).

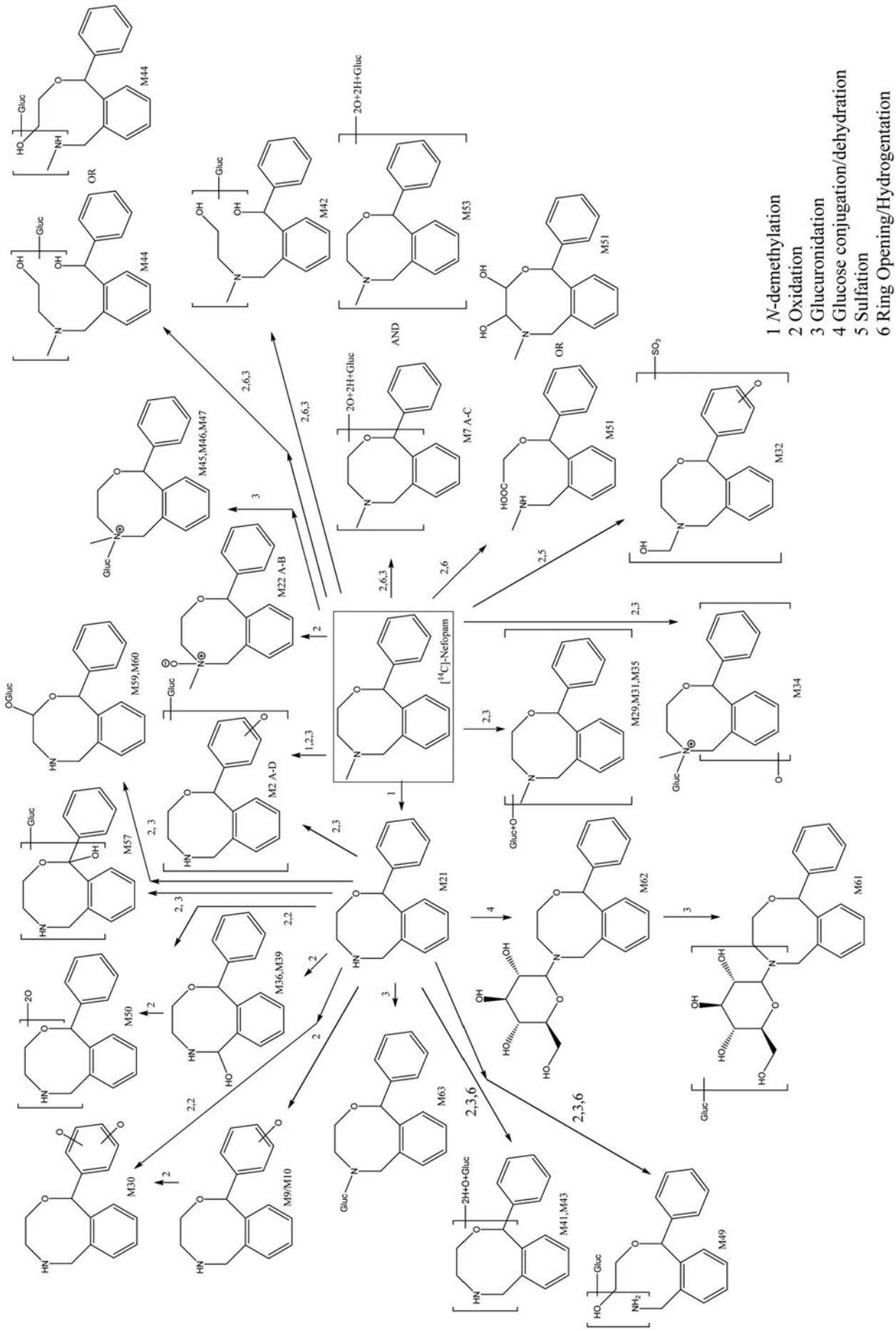

Figure 7. Proposed metabolic scheme for the biotransformation of [^{14}C]-nefopam in humans.

Acknowledgements

The authors thank Drs. Gopal Damodara and Jason Smulik at Ricerca Biosciences for synthesis of radiolabeled nefopam; Xiaohong Liu, James Pombier, Sara Wills, Lori Joas, and Mike Potchoiba at Covance Laboratories for help with conduct and analysis of the study; Eric Solon at QPS for estimating human radiation dosimetry; and Weiru Hong at Impax for assistance with the clinical conduct of the study.

Declaration of interest

The authors report no conflicts of interest. The authors alone are responsible for the content and writing of this article.

A. Mittur and Nishit B. Modi are employees of Impax Laboratories, Inc. and hold Impax stock.

References

Aymard G, Warot D, Démolis P, et al. (2003). Comparative pharmacokinetics and pharmacodynamics of intravenous and oral nefopam in healthy volunteers. Pharmacol Toxicol 92:279–86.

Bolt AG, Graham G, Wilson P. (1974). Stereoselective demethylation of the enantiomers of nefopam, an experimental antidepressant and skeletal muscle relaxant. Xenobiotica 4:355–63.

Chawla J, Le Guern ME, Alquier C, et al. (2003). Effect of route of administration on the pharmacokinetic behavior of enantiomers of nefopam and desmethylnefopam. Ther Drug Monit 25:203–10.

Dell'Osso B, Buoli M, Baldwin DS, Altamura AC. (2010). Serotonin norepinephrine reuptake inhibitors (SNRIs) in anxiety disorders: a comprehensive review of their clinical efficacy. Hum Psychopharmacol 25:17–29.

Evans MS, Lysakowski C, Tramer MR. (2008). Nefopam for the prevention of postoperative pain: quantitative systematic review. Br J Anaesth 101:610–17.

Girard P, Coppé MC, Verniers D, et al. (2006). Role of catecholamines and serotonin receptor subtypes in nefopam-induced antinociception. Pharmacol Res 54:195–202.

Heel RC, Brogden RN, Pakes GE, et al. (1980). Nefopam: a review of its pharmacological properties and therapeutic efficacy. Drugs 19: 249–67.

Hop CE, Wang Z, Chen Q, Kwei G. (1998). Plasma-pooling methods to increase throughput for *in vivo* pharmacokinetic screening. J Pharm Sci 87:901–3.

Houston JB, Taylor G. (1984). Drug metabolite concentration–time profiles: influence of route of drug administration. Br J Clin Pharmacol 17:385–94.

Hunskaar S, Fasmer OB, Broch OJ, Hole K. (1987). Involvement of central serotonergic pathways in nefopam-induced antinociception. Eur J Pharmacol 138:77–82.

Kapfer B, Alfonsi P, Guignard B, et al. (2005). Nefopam and ketamine comparably enhance postoperative analgesia. Anesth Analg 100: 169–74.

Kirchherr HJ, Christ W. (1984). Nefopam and *N*-desmethyl-nefopam: activity in the hot plate and writhing test. Naunyn Schmiedebergs Arch Pharmacol 325:R72.

Lee YC, Chen PP. (2010). A review of SSRIs and SNRIs in neuropathic pain. Expert Opin Pharmacother 11:2813–25.

Mimoz O, Chauvet S, Grégoire N, et al. (2010). Nefopam pharmacokinetics in patients with end-stage renal disease. Anesth Analg 111: 1146–53.

Mulder GJ. (1992). Glucuronidation and its role in regulation of biological activity of drugs. Annu Rev Pharmacol Toxicol 32:25–49.

Novelli A, Diaz-Trelles R, Groppetti A, Fernandez-Sanchez MT. (2005). Nefopam inhibits calcium influx, cGMP formation, and NMDA receptor-dependent neurotoxicity following activation of voltage sensitive calcium channels. Amino Acids 28:183–91.

Rydberg P, Gloriam DE, Zaretzki J, et al. (2010). SMARTCyp: a 2D method for prediction of cytochrome P450-mediated drug metabolism. ACS Med Chem Lett 1:96–100.

Taylor D, Lenox-Smith A, Bradley A. (2013). A review of the suitability of duloxetine and venlafaxine for use in patients with depression in primary care with a focus on cardiovascular safety, suicide and mortality due to antidepressant overdose. Ther Adv Psychopharmacol 3:151–61.

Thase ME. (2008). Are SNRIs more effective than SSRIs? A review of the current state of the controversy. Psychopharmacol Bull 41: 58–85.

Verleye M, André N, Heulard I, Gillardin JM. (2004). Nefopam blocks voltage-sensitive sodium channels and modulates glutamatergic transmission in rodents. Brain Res 1013:249–55.